# Guided elastic waves in porous materials saturated by air under Lamb conditions

Laurens Boeckx, Philippe Leclaire, Poonam Khurana, Christ Glorieux, Walter Lauriks, Jean-François Allard

# Guided elastic waves in porous materials saturated by air under Lamb conditions

L. Boeckx, P. Leclaire, P. Khurana, C. Glorieux,[a] and W. Lauriks[b]
*Laboratorium voor Akoestiek en Thermische Fysica, Katholieke Universiteit Leuven, Celestijnenlaan 200D, B-3001 Heverlee, Belgium*

J. F. Allard
*Laboratoire d'Acoustique de l'Université du Maine, Unité Mixte de Recherche du Centre National de la Recherche Scientifique (UMR CNRS) 6613, Avenue Olivier Messiaen, 72085 Le Mans Cédex, France*

The propagation of guided elastic waves in porous materials saturated by air under Lamb conditions is studied theoretically and experimentally. The modes are derived from expressing the boundary conditions on the normal and tangential stresses and the displacements at the interfaces between the porous layer and the surrounding fluid. The stresses and the fluid pressure inside the porous medium are obtained from Biot's equations of poroelasticity. Symmetrical and antisymmetrical modes are found when the porous layer is loaded by the same fluid on both sides. Damping mechanisms include viscous and thermal exchanges between the solid and the fluid, in addition to the classical structural damping. Using an experimental setup based on the generation of standing waves in the layer and taking the spatial Fourier transform of the displacement profile, the phase velocities of three modes were measured for two porous materials in a frequency range between 80 Hz and 4 kHz. The measurements confirm the theoretical predictions and provide information on the shear modulus of a sound-absorbing material in a wide frequency range.

## I. INTRODUCTION

Surface waves at the interface between a solid and a fluid and guided waves in layers of solid have long been established as important tools for determining material properties (see Refs. 1,2). For porous materials, theoretical and experimental studies of surface waves were presented for liquid-saturated media,[3,4] in materials saturated by air for applications in outdoor sound propagation,[5,6] and for material characterization in highly porous absorbent materials saturated by air at ultrasonic frequencies.[7,8] In air-saturated materials, the solid is generally more rigid and heavier than air, and the study of surface waves is often restricted to the wave propagating in the air above the porous interface in the rigid frame approximation. More recently, Allard *et al.*[9] have studied the structure-borne surface wave in soft porous materials, with the determination of the shear modulus at very high frequencies as a direct application. Making the link with laser ultrasonics for material characterization, Allard *et al.*[10] studied the deformation and phase velocities of laser-induced surface waves at a fluid-saturated porous interface in the Rayleigh wave regime. The transmission and reflection coefficients of water-saturated porous plates were also studied theoretically by Belloncle *et al.*[11] More recently, Boeckx *et al.*[12] presented a theoretical and experimental study of the guided modes in thin porous layers lying on a rigid substrate and saturated by air. It was found that two sets of guided waves can propagate in a porous layer: the structure-borne guided waves, with the Rayleigh and the shear velocities as high-frequency limits, and the fluid-borne guided waves, with the velocity of Biot's wave of the second kind as the high-frequency limit. An experimental principle for the detection of these waves in highly damping materials was suggested. The main contribution of this work to the mechanical characterization of porous materials was the possibility to access the intermediate frequency range (200 Hz–1.5 kHz, typically) between the frequencies described by classical transfer function methods[13,14] at low frequencies and the Rayleigh wave characterization[9] in the high-frequency limit.

In this article, guided waves in porous layers under Lamb conditions are studied and a new experimental configuration is proposed. The modes are derived by using displacement potentials to derive the normal and tangential stresses and by expressing the boundary conditions at the interfaces between the porous layer and the surrounding fluid. The stresses and the fluid pressure inside the porous medium are obtained from Biot's equations of poroelasticity.[15] Symmetrical and antisymmetrical modes are found in a porous medium if the layer is loaded by the same fluid on both sides. The materials studied exhibit high structural damping, and complex elastic moduli have to be used. In addition, the viscous and thermal interactions between the solid and the fluid are included in the model. An experimental setup based on the generation of standing waves in a plate of finite size is proposed for the measurement of the phase velocities of porous layers under Lamb conditions. The phase velocities for two different materials are measured be-

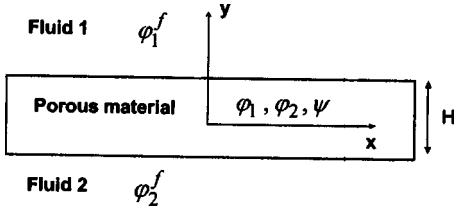


FIG. 1. Layer of material under Lamb conditions and system of coordinates.

tween 80 Hz and 4 kHz. The experimental results are compared with the model and provide information on the shear modulus of a sound-absorbing material in a wide frequency range that is difficult to access with classical methods.

## II. GUIDED WAVES IN A POROUS LAYER SATURATED BY A FLUID UNDER LAMB CONDITIONS

### A. Displacement potentials

In the following, the dispersion equation of the guided waves in a porous layer with open pores under Lamb conditions are derived from the displacement potentials, the expressions for the displacements, stresses, and the boundary conditions. A porous plate of thickness $H$ is loaded on both sides with two different fluids in the general case (Fig. 1). The wave propagation in the porous medium is described by two scalar potentials $\varphi_1$ and $\varphi_2$ associated with two compressional waves and by one vector potential, which is associated with a shear wave and whose only nonzero component $\psi$ is on the $z$ axis. The potentials $\varphi_1^f$ and $\varphi_2^f$ are defined for compressional waves in the surrounding fluids. These potentials satisfy the equations of propagation

$$\nabla^2\varphi_1 - \frac{1}{V_{L_1}^2}\partial_t^2\varphi_1 = 0, \tag{1a}$$

$$\nabla^2\varphi_2 - \frac{1}{V_{L_2}^2}\partial_t^2\varphi_2 = 0, \tag{1b}$$

$$\nabla^2\psi - \frac{1}{V_T^2}\partial_t^2\psi = 0 \tag{1c}$$

and

$$\nabla^2\varphi_1^f - \frac{1}{V_{F_1}^2}\partial_t^2\varphi_1^f = 0, \tag{2a}$$

$$\nabla^2\varphi_2^f - \frac{1}{V_{F_2}^2}\partial_t^2\varphi_2^f = 0, \tag{2b}$$

where $V_{L_1}$ and $V_{L_2}$ are the velocities of the two Biot compressional waves[15] and $V_T$ the velocity of the Biot shear wave. $V_{F_1}$ and $V_{F_2}$ are the free velocities in the surrounding fluids. The Biot velocities are obtained from

$$\frac{1}{V_{L_1}^2} = \frac{1}{2}\frac{P\rho_{22} + R\rho_{11} - 2Q\rho_{12}}{PR - Q^2}\left[1 \pm \left(1 - 4 \times \frac{(PR - Q^2)(\rho_{11}\rho_{22} - \rho_{12}^2)}{(P\rho_{22} + R\rho_{11} - 2Q\rho_{12})^2}\right)^{1/2}\right], \quad i = 1,2 \tag{3}$$

$$V_T = \sqrt{\frac{N_s}{(1-\phi)\rho_s + \left(1 - \frac{1}{\alpha_\infty}\right)\phi\rho_f}}, \tag{4}$$

where $\phi$ is the porosity, $\alpha_\infty$ is the tortuosity, $\rho_s$ and $\rho_f$ are the densities of the solid and of the fluid, respectively, $\rho_{11}, \rho_{12}$, and $\rho_{22}$ are the elements of a density matrix;[15] $N_s$ is the shear modulus of the porous frame, and $P, Q$, and $R$ are the elastic coefficients defined by Biot and Willis[16] for a fluid-saturated porous medium. These coefficients are functions of the bulk modulus of the solid $K_s$, of the porous frame $K_b$, and of the fluid $K_f$. The attenuation by viscous friction can be included by using a complex tortuosity function $\alpha(\omega)$ to replace $\alpha_\infty$.[17] The thermal exchanges can be accounted for through the use of a frequency-dependent elastic modulus $K_f$.[18] The potentials are functions of the direction of propagation $x$, of the direction perpendicular to the direction of propagation $y$, and of the time $t$ Harmonic solutions are chosen in time and in $x$. For the dependence along the $y$ axis, the linear combination of hyperbolic sines and cosines proposed by Ewing *et al.*,[19] is chosen for the potentials in the porous layer. The motivation for this choice is that true symmetrical and antisymmetrical modes do not exist in a plate loaded with two different fluids on either side, and a general form is chosen. As it will be shown in Sec. II C, the symmetry of the plate when surrounded by a single fluid will result in the exsistence of symmetrical and antisymmetrical modes. The two families of dispersion curves corresponding to symmetrical and antisymmetrical modes are decoupled can cross each other.[20] The potentials in the porous medium and the two potentials in the fluid are written as

$$\varphi_1 = \big(A_1\cosh(p_1 y) + A_2\sinh(p_1 y)\big)e^{i(\omega t - kx)}, \tag{5}$$

$$\varphi_2 = \big(B_1\cosh(p_2 y) + B_2\sinh(p_2 y)\big)e^{i(\omega t - kx)}, \tag{6}$$

$$\psi = \big(C_1\cosh(qy) + C_2\sinh(qy)\big)e^{i(\omega t - kx)}, \tag{7}$$

$$\varphi_1^f = D_1 e^{-\gamma_1 y}e^{i(\omega t - kx)} \quad \text{for} \quad y \geqslant \frac{H}{2}, \tag{8}$$

$$\varphi_2^f = D_2 e^{\gamma_2 y}e^{i(\omega t - kx)} \quad \text{for} \quad y \leqslant -\frac{H}{2}, \tag{9}$$

where $A_1, A_2, B_1, B_2, C_1, C_2, D_1$, and $D_2$ are constants, $\omega$ is the angular frequency, $p_{1,2}, q$, and $\gamma_{1,2}$ are the $y$ components of the wave numbers for the different potentials, and $k$ is their common $x$ component. Upon inserting the expressions for the potentials in the equations of propagation (1) and (2), the following relations are found:

$$P_{1,2}^2 - k^2 + \frac{\omega^2}{V_{L_{1,2}}^2} = 0, \tag{10}$$

$$q^2 - k^2 + \frac{\omega^2}{V_T^2} = 0, \tag{11}$$

$$\gamma_{1,2}^2 - k^2 + \frac{\omega^2}{V_{F_{1,2}}^2} = 0. \tag{12}$$

Conditions on the imaginary parts of $k$ and of $\gamma_{1,2}$ must be fulfilled for the guided waves in the material to be physical.[12] Also, the real part of $\gamma_{1,2}$ will determine whether the modes radiate energy in the surrounding fluids 1 and 2 (leaky Lamb modes) or the fluid waves are localized near the interfaces.

### B. Boundary conditions on stresses and normal displacement

The boundary conditions on the normal and tangential stresses at $y = \pm H/2$ are given by

$$\sigma_{yy}^f = -\phi P_{1,2}, \tag{13}$$

$$\sigma_{yy}^s = -(1-\phi)P_{1,2}, \tag{14}$$

$$\sigma_{xy}^s = 0, \tag{15}$$

where $P_{1,2}$ are the pressures exerted by the surrounding fluids 1 and 2 at $y = \pm H/2$, and $\sigma_{yy}^f$ and $\sigma_{yy}^s$ are the Biot stresses along the $y$ axis for the effective fluid in the porous medium and the solid frame. An additional boundary condition is given by the continuity of the normal components of the displacements at the interfaces between the porous media and the surrounding fluids at $y = \pm H/2$

$$(1-\phi)u_y + \phi U_y = U_{y_{1,2}}^F, \tag{16}$$

where $u_y$ and $U_y$ are the normal components of the solid and fluid displacements **u** and **U** in the porous medium, respectively, and $U_{y_{1,1}}^F$ is the normal component of the displacement in the surrounding fluid.

### C. Determinant of the boundary conditions

The Biot stresses are given by

$$\sigma_{yy}^s = \left[(P - 2N_s + \mu_1 Q)\left(p_1^2 - k^2\right) + 2N_s p_1^2\right]\varphi_1 + \left[(P - 2N_s + \mu_2 Q)\left(p_2^2 - k^2\right) + 2N_s p_2^2\right]\varphi_2 + j2N_s k\partial_y \psi, \tag{17}$$

$$\sigma_{yy}^f = (Q + \mu_1 R)\left(p_1^2 - k^2\right)\varphi_1 + (Q + \mu_2 R)\left(p_2^2 - k^2\right)\varphi_2, \tag{18}$$

$$\sigma_{xy}^s = 2N_s\left[-jk\partial_y\varphi_1 - jk\partial_y\varphi_2 + \frac{1}{2}\left(q^2 + k^2\right)\psi\right], \tag{19}$$

where the coefficients $\mu_1, \mu_2$, and $\mu_3$ correspond to the amplitude ratios of the waves in the porous material.[9]

$$\mu_i = \frac{Pk_i - \omega^2\rho_{11}}{\omega^2\rho_{12} - Qk_i}, \quad i = 1,2 \tag{20}$$

$$\mu_3 = \frac{\rho_{12}}{\rho_{22}}. \tag{21}$$

Inserting the potentials (5)–(9) into the boundary conditions (13)–(16) for both sides of the plate yields a system of eight equations with the eight unknowns $A_1, A_2, B_1, B_2, C_1, C_2, D_1$, and $D_2$. The relation between $\omega$ and $k$, i.e., the equation of dispersion is obtained by equating the determinant of this system to zero

$$\begin{vmatrix}
-jkp_1s_1 & -jkp_1c_1 & -jkp_2s_2 & -jkp_2c_2 & \frac{1}{2}(k^2+q^2)c_q & \frac{1}{2}(k^2+q^2)s_q & 0 & 0 \\
M_1c_1 & M_1s_1 & M_2c_2 & M_2s_2 & 0 & 0 & -\phi P_1 & 0 \\
N_1c_1 & N_1s_1 & N_2c_2 & N_2s_2 & j2N_skqs_q & j2N_skqc_q & -(1-\phi)P_1 & 0 \\
K_1s_1 & K_1c_1 & K_2s_2 & K_2c_2 & K_3c_q & K_3s_q & \gamma_1 e^{-\gamma_1 H/2} & 0 \\
jkp_1s_1 & -jkp_1c_1 & jkp_2s_2 & -jkp_2c_2 & \frac{1}{2}(k^2+q^2)c_q & -\frac{1}{2}(k^2+q^2)s_q & 0 & 0 \\
M_1c_1 & -M_1s_1 & M_2c_2 & -M_2s_2 & 0 & 0 & 0 & -\phi P_2 \\
N_1c_1 & -N_1s_1 & N_2c_2 & -N_2s_2 & -j2N_skqs_q & j2N_skqc_q & 0 & -(1-\phi)P_2 \\
-K_1s_1 & K_1c_1 & -K_2s_2 & K_2c_2 & K_3c_q & -K_3s_q & 0 & -\gamma_2 e^{-\gamma_2 H/2}
\end{vmatrix} = 0 \tag{22}$$

with

$$M_1 = (R + \mu_1 Q)\left(p_1^2 - k^2\right),$$

$$M_2 = (R + \mu_2 Q)\left(p_2^2 - k^2\right),$$

$$N_1 = (P - 2N_s + \mu_1 Q)\left(p_1^2 - k^2\right) + 2N_s p_1^2,$$

$$N_2 = (P - 2N_s + \mu_2 Q)\left(p_2^2 - k^2\right)2N_s p_2^2,$$

$$K_1 = [(1-\phi) + \mu_1\phi]p_1,$$

$$K_2 = [(1-\phi) + \mu_2\phi]p_2,$$

$$K_3 = jk[(1-\phi) + \mu_3\phi],$$

$$P_1 = K_{f_1}\left(\gamma^2 - k^2\right)e^{-\gamma_1 H/2},$$

$$P_2 = K_{f_2}\left(\gamma^2 - k^2\right)e^{-\gamma_2 H/2},$$

$$s_1 = \sinh\left(p_1 H/2\right),$$

$$s_2 = \sinh(p_2 H/2),$$

$$s_q = \sinh(qH/2),$$

$$c_1 = \cosh(p_1 H/2),$$

$$c_2 = \cosh(p_2 H/2),$$

$$c_q = \cosh(qH/2).$$

This determinant describes the dispersion of guided waves in a porous layer with open pores and surrounded by two different fluids 1 and 2. An example of such a situation could be a porous layer immersed in water in a tank and with the upper surface coinciding with the interface between water and air. In this case, the saturating fluid would be water. In the case where the two surrounding fluids and the fluid in the pores are the same,

$$\gamma_1 = \gamma_2 = \gamma \text{ and } P_1 = P_2 = P. \tag{23}$$

It is interesting to notice the symmetry in determinant (22). Discarding the last two columns, one can notice that the last four rows are obtained from the first four rows by changing the signs of the coefficients involving the hyperbolic sines ($s_1, s_2$, and $s_q$). This property can be used to write this determinant in a different way. By adding and subtracting rows, it is possible to create new rows without changing the determinant. It is also possible to create new columns without changing the determinant by adding or subtracting columns. This property is related to the fact that transposing a determinant does not change its value. Using these properties and if conditions (23) are fulfilled, it is possible to write the determinant (22) in the following form:

$$\begin{vmatrix}
-2jkp_1c_1 & -2jkp_2c_2 & (k^2+q^2)c_q & 0 & 0 & 0 & 0 & 0 \\
2M_1s_1 & 2M_2s_2 & 0 & -2\phi P & 0 & 0 & 0 & 0 \\
2N_1s_1 & 2N_2s_2 & j4N_skqs_q & -2(1-\phi)P & 0 & 0 & 0 & 0 \\
2K_1c_1 & 2K_2c_2 & 2K_3c_q & 2\gamma e^{-\gamma H/2} & 0 & 0 & 0 & 0 \\
0 & 0 & 0 & 0 & -2jkp_1s_1 & -2jkp_2s_2 & (k^2+q^2)s_q & 0 \\
0 & 0 & 0 & 0 & 2M_1c_1 & 2M_2c_2 & 0 & -2\phi P \\
0 & 0 & 0 & 0 & 2N_1c_1 & 2N_2c_2 & j4N_skqc_q & -2(1-\phi)P \\
0 & 0 & 0 & 0 & 2K_1s_1 & 2K_2s_2 & 2K_3s_q & 2\gamma e^{-\gamma H/2}
\end{vmatrix} = 0. \tag{24}$$

This determinant is block diagonal, and the equation of dispersion is finally written as the product of two $4\times4$ determinants

$$\begin{vmatrix}
-2jkp_1c_1 & -2jkp_2c_2 & (k^2+q^2)c_q & 0 \\
2M_1s_1 & 2M_2s_2 & 0 & -2\phi P \\
2N_1s_1 & 2N_2s_2 & j4N_skqs_q & -2(1-\phi)P \\
2K_1c_1 & 2K_2c_2 & 2K_3c_q & 2\gamma e^{-\gamma H/2}
\end{vmatrix} \times \begin{vmatrix}
-2jkp_1s_1 & -2jkp_2s_2 & (k^2+q^2)s_q & 0 \\
2M_1c_1 & 2M_2c_2 & 0 & -2\phi P \\
2N_1c_1 & 2N_2c_2 & j4N_skqc_q & -2(1-\phi)P \\
2K_1s_1 & 2K_2s_2 & 2K_3s_q & 2\gamma e^{-\gamma H/2}
\end{vmatrix} = 0. \tag{25}$$

Plotting the dispersion curves associated with the two $4\times4$ determinants shows that the first determinant of the left-hand side of Eq. (25) corresponds to antisymmetrical modes in porous layers, while the second corresponds to symmetrical modes. The solutions are obtained by splitting Eq. (25) into two equations involving the first and second $4\times4$ determinants successively. It is also worth noticing that the two $4\times4$ determinants can be deduced from one another by interchanging the hyperbolic sines and cosines.

### D. Dispersion curves

The phase velocity curves for a highly porous foam (foam 1) were calculated and are shown in Fig. 2. The material properties used are given in Table I. The same numerical algorithm as the one described in Ref. 12 was used to solve Eq. (25). The velocities of the three Biot waves were calculated using Eqs. (3) and (4) in which the parameters are obtained from Refs. 15, 16, and 12 and from Table I. It can be noticed that for some modes, the dispersion curves are similar to those obtained from the Lamb theory for an elastic solid. $A_0$ and $S_0$ modes for porous media can be identified at low frequencies. The disappearance of cutoff frequencies and the presence of maxima that can be observed for modes of higher order are a consequence of the inclusion of damping mechanisms in the models. These are the classical structural damping associated with the complex elastic moduli and Biot's attenuation mechanisms. The imaginary parts of the wave numbers, i.e., the attenuations [Fig. 2(b)], are very useful for the prediction of the modes that can be observed and the frequency regions where they should be detected. In the frequency range investigated, the modes that are likely to be observed are those with the smallest imaginary parts, namely, $A_0, S_0$, and $A_1$. The parts of other modes should also be observable when their imaginary parts are low.

As for the Melamine foam studied in Ref. 12, a second set of dispersion curves is predicted. The existence of two

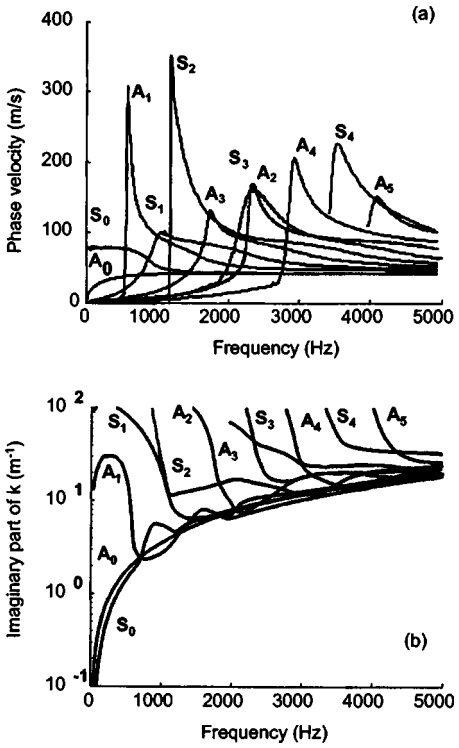


FIG. 2. Theoretical dispersion curves for guided waves in a porous material (foam 1). (a) Real parts of the phase velocities and (b) imaginary parts of the wave numbers.

sets of dispersion curves is associated with the two scalar potentials $\varphi_1$ and $\varphi_2$ and is a consequence of the existence of two compressional and one shear waves in the porous medium. The second set could be plotted as well as the first set by solving Eq. (25). Only the structure-borne dispersion curves are presented in the frequency range studied. Plotting the second set at frequencies higher than those studied here would show that the velocity of Biot's wave of the second kind acts as a limit velocity (see also Fig. 7 in Ref. 12 and comments therein). In Ref. 12, the second set of dispersion curves could be distinguished when the curves were calculated up to 10 kHz. For the foam studied in Fig. 2, the permeability is approximately 10 times lower than the permeability of the Melamine foam. The characteristic frequency separating the low- and high-frequency regimes is then 10 times higher. It is predicted, and it could be verified, that the limit velocity for the second set of dispersion curves is observable at around 100 kHz and above. These frequencies could not be reached experimentally in this study.

TABLE I. Material properties.

| | Foam 1 | Foam 2 |
|---|---|---|
| Tortuosity $\alpha_\infty$ | 1.4 | 1.1 |
| Flow resistivity $\sigma$(Ns/m$^4$) | 130 000 | 5000 |
| Viscous dimension $\Lambda(\mu$m) | 60 | 50 |
| Thermal dimension $\Lambda'(\mu$m) | 180 | 150 |
| Density $\rho$(kg/m$^3$) | 59 | 32 |
| Porosity $\phi$ | 0.98 | 0.98 |
| Thickness $H$ (m) | 0.04 | 0.05 |
| Shear modulus $N_s$ (kPa) | $127+12.7i$ | $61+6.1i$ |

## III. EXPERIMENTAL CONFIGURATION

### A. Wave excitation in highly damping materials

A difficulty one faces when studying structure-borne waves in porous polyurethane foams is the high level of structural damping. In addition, significant attenuation is introduced by the viscous frictions and thermal exchanges between the solid and the fluid. The short-pulse propagation method in layers of infinite extent and a time-frequency analysis to obtain the dispersion curve, a standard method used in laser ultrasonics, can hardly be implemented as the waves are rapidly damped, and there is not enough energy per frequency to obtain sensible results. In order to supply more energy per frequency, an excitation with sine bursts is possible, and the detection can take place at longer distances. Results of experiments on guided waves using sine bursts are reported in Ref. 21. Several modes could be detected at particular frequencies where the velocities of the different modes are very different. The main disadvantage of this method is that it requires bursts with fairly large duration in order to excite the material with enough energy and with a narrowband signal. The only situation where it is possible to eventually observe several guided modes is, therefore, when the velocities are very different. This occurs in limited frequency regions only. In regions where two modes have similar velocities, the bursts overlap and it is not possible to distinguish the different modes. Time-frequency analysis for separating the modes cannot be used as the source is narrowband.

### B. Experimental principle

The method proposed here for measuring the phase velocities of the guided waves is based on the generation of standing waves in the layer excited harmonically at frequencies that can be varied and on the spatial Fourier transform of the standing-wave pattern to identify the different guided modes. It is similar in principle to the standing-wave tube method for measuring the acoustical properties of materials that uses the reflection of the incident wave to create a standing-wave field in the tube. This principle has been used by Kelders *et al.*[22] in surface-wave propagation experiments above a periodical grating at ultrasonic frequencies. The key advantages of this method are that more energy can be supplied at a given frequency when harmonic excitation is used, the signals do not need to be localized in time, and the standing-wave pattern can be determined simply by scanning the surface of the layer along the direction of propagation. The spatial Fourier transform of the surface profile detects all spatially periodic components and provides the wave numbers $k_j$ of different modes propagating in the layer at the angular frequency $\omega$. The phase velocities of the different modes indexed $j$ are then given by

$$V_j(\omega) = \frac{\omega}{k_j}. \tag{28}$$

The spatial spectrum obtained from the Fourier transform provides information not only on the spatial frequencies of the modes but also on their damping.

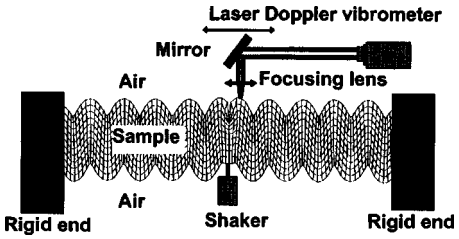


FIG. 3. Finite element simulation of the deformation at 200 Hz of an undamped elastic plate, with the effective properties of the porous layer saturated by air under Lamb conditions (foam 1), for a line source located at the center.

### C. Experimental setup

Although the principle is the same as that used in Ref. 12, the experimental configuration is different. The configuration is shown in Fig. 3, where a layer of porous material is mounted under symmetrical conditions with its two ends glued to thick metal plates to achieve rigid endings at which the waves are perfectly reflected (the porous material is much softer and lighter than the metal ends). The porous sample was excited harmonically at the center with the help of a line source. In order to generate plane waves propagating along the $x$ axis, a thin metal plate attached to a shaker was used as a line source. In Fig. 3, the displacement profile of an elastic plate with the effective properties of a porous plate (foam 1) was calculated at 200 Hz with the help of a finite element code (FEM). The FEM was used to visualize the standing-wave pattern obtained from the wave reflections at the rigid ends, for any configuration of the source. The main advantages of this new experimental condition are that the standing-wave pattern is expected to be symmetrical about the vertical plane that cuts the plate in two equal halves, displacements at the rigid ends are zero such that the periodization of the pattern in the numerical implementation of the Fourier transform does not introduce discontinuities, and no spatial windowing is required. The main disadvantages are that very soft material will tend to sag when glued on both extremities to the rigid backings and that the excitation and the detection take place on opposite sides, which may reduce the measurable high-frequency limit. The line source attached to the sample and a slight tension applied to the sample can help to reduce the sagging. The shaker driving the source was fed with a continuous sine function provided by the function generator unit of a SRS SR780 two-channel signal analyzer. At each driving frequency of the source, the displacement of the surface was measured using a laser Doppler vibrometer. The detection method is the same as in Ref. 12 and is summarized in Fig. 3. Typical measurement steps between 1 and 5 mm in the measurement path were used. The amplitude and phase of the response of the surface were measured using the lock-in amplifier of the signal analyzer. The entire setup was automated and placed in a semianechoic chamber.

### D. Experimental results on the standing-wave patterns

Examples of measured standing-wave patterns for foam 1 and their spectra are shown in Fig. 4. The measurements were performed at a temperature of 21 °C and variations remained within 5% of this value. Figures 4(a)–4(c) show the standing-wave patterns at 202, 600, and 800 Hz, respectively, while Figs. 4(d)–4(f) show their respective spatial spectra. At low frequency, only the $A_0$ mode could be observed, as only one clear peak was present for frequencies between 50 and 400 Hz (this becomes clear when plotting the experimental results on the phase velocities and comparing with the predictions). The $S_0$ mode is generally more difficult to excite and to detect at low frequencies. With increasing frequency, a maximum related to the $S_0$ mode appears in the spectrum of the standing-wave pattern. At 800 Hz a high-wavelength periodicity is present in the standing-wave pattern corresponding to a higher-frequency mode, which was identified as $A_1$. The excitation of the standing-wave pattern at even higher frequencies becomes increasingly difficult due to greater attenuation and to the fact that the excitation and the detection are on opposite sides. The high-frequency behavior can nonetheless be estimated from the asymptotical behavior of the modes. High-excitation amplitudes and increasing detection accuracy are needed, but are limited by the possible source overheating and nonlinear effects of the material localized near the source.

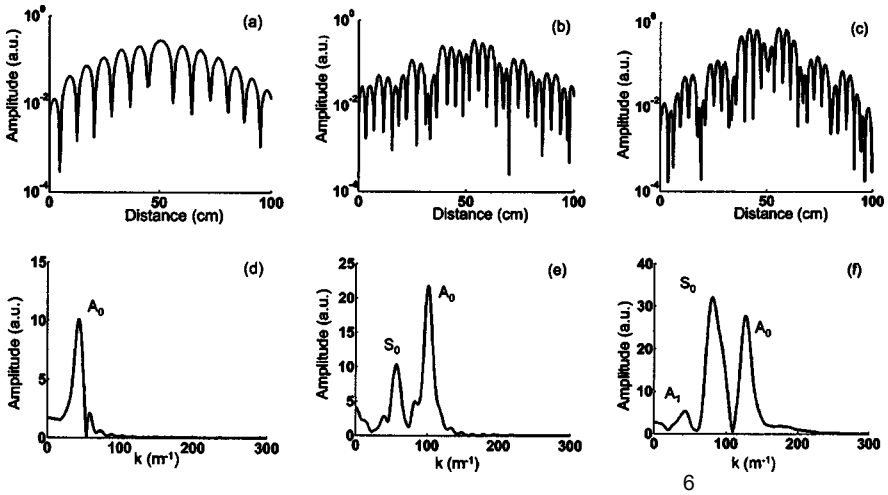


FIG. 4. (a), (b) and (c): Experimental standing-wave patterns. (d), (e) and (f): Spatial Fourier transforms of the measured standing-wave patterns. (a) and (d), 202 Hz; (b) and (e), 600 Hz; (c) and (f), 800 Hz.

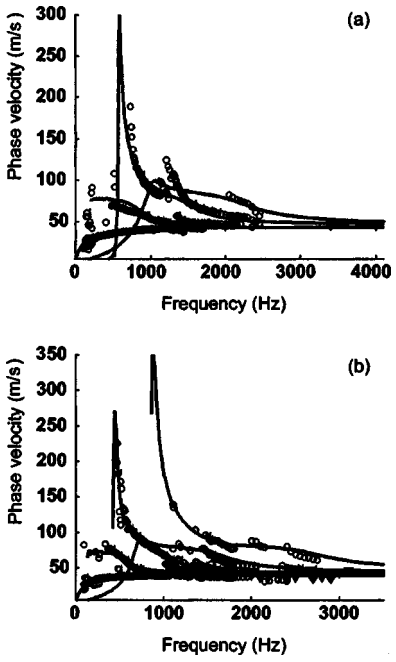


FIG. 5. Experimental results on the phase velocities of guided waves in highly porous foams saturated by air and comparison with theoretical predictions. (a) Foam 1 and (b) foam 2. The triangles correspond to Rayleigh-wave velocity measurements (Ref. 9).

## IV. EXPERIMENTAL RESULTS ON THE PHASE VELOCITIES AND COMPARISON WITH THE PREDICTIONS

The phase velocities of two highly porous materials were investigated using the setup and the principle described in the previous sections. The first sample (foam 1) is a material of which the rigidity has already been studied using an acoustical technique described in Ref. 23. In this paper the phase velocity of the Rayleigh-wave regime was determined to be around $V_{\mathrm{Rayl}}=44$ m/s, which corresponded to a shear modulus of 125 kPa for a Poisson ratio of 0.3. The measurements of the Rayleigh-wave velocity were performed at 2, 3.4, and 4 kHz. At low frequencies, the behavior was verified with a classical springlike resonance test, which provided a value for the shear modulus of 130 kPa for a resonance frequency at 37 Hz. The experimental and calculated phase velocities for the two foams are presented in Fig. 5(a) and 5(b). The triangles indicate Rayleigh-wave velocity measurements performed at different frequencies. The Biot parameters used for the calculation were measured using standard techniques and are given in Table I. A fitting algorithm was used in order to obtain a frequency dependence of the shear modulus. First, the algorithm was tested by fitting the experimental data with a theoretical $A_0$ mode in which the shear modulus had a known frequency dependence. Random noise was added to the data. For both samples, a structural damping of 5% and a Poisson ratio of 0.3 were used. It was found that within the limits of the random noise, the fitting algorithm was able to reproduce the frequency dependence of the shear modulus supplied initially. The fitting algorithm seemed far less sensitive to variations in the Poisson ratio and damping rates. The measured Rayleigh velocity was used as a starting value for the fit. The fitting algorithm also proved to be rather insensitive to reasonable variations in the starting values. After the fitting was checked, the true frequency variations of the shear modulus were determined from the theoretical model of Sec. II in which the shear modulus was a free parameter. The variations of the shear modulus of around 10% were found for the first sample, and of 5% for the second sample in the frequency range studied. These variations are fairly small and for this reason, it was decided to do the comparison between theoretical and experimental results with a constant value of the shear modulus. The values used in the model were 127 kPa for the first sample and 61 kPa for the second sample. The good correspondence between the theoretical and experimental results seems to provide evidence that the $S_0$ and $A_1$ modes were detected and measured. In Fig. 5(a), however, a larger difference between theoretical and experimental results can be observed at around 700 Hz. This can be explained by the fact that the measurement error is higher for higher phase velocities. Assuming no error on the frequency and referring to Eq. (28),

$$\left|\frac{\Delta V}{V}\right| = \left|\frac{\Delta k}{k}\right|. \tag{29}$$

Since $\Delta k$ can be considered fairly constant throughout the spatial frequency range, the ratio $|\Delta V/V|$ is higher for smaller values of $k$. The very dispersive part of a higher-order mode is therefore difficult to trace accurately. In addition, Fig. 2(b) shows that the damping of the modes increases near a cutoff frequency, making the modes more difficult to detect and increasing the measurement error. Another important source of error is the large width of the peaks in the spatial spectrum and the different amplitudes of the modes. The spectrum is dominated throughout a large frequency domain by the $A_0$ mode, making the estimation of phase velocities corresponding to smaller maxima in the spectrum less accurate. The crossing of dispersion curves is described with less accuracy due to the width of the peaks. The detection system is such that modes for which the displacement of matter is mainly parallel to the surface of the layer will be detected with less accuracy. Sagging of the sample and anisotropy should also be mentioned as possible sources of error.

## V. CONCLUSION

A theoretical and experimental study of the propagation of guided waves in air-saturated porous layers under Lamb conditions was presented. It was shown in Ref. 12 and confirmed in this article that two sets of guided waves can propagate in the layer. The existence of symmetrical and antisymmetrical modes was predicted for a sample saturated and loaded on both sides by the same fluid. A clear experimental evidence was found for the propagation of three modes ($A_0, S_0$, and $A_1$) and these compared very well with the theoretical predictions. This study demonstrates the possibility to determine variations of the shear modulus in a wide frequency range from 80 Hz up to 4 kHz.

[1]D. E. Chimenti, Appl. Mech. Rev. **50**, 247 (1997).
[2]C. Glorieux *et al.*, Rev. Sci. Instrum. **74**, 465 (2003).
[3]H. Deresiewicz, Bull. Seismol. Soc. Am. **52**, 627 (1962).

[4]S. Feng and D. L. Johnson, J. Acoust. Soc. Am. **74**, 906 (1983).
[5]K. Attenborough, J. Acoust. Soc. Am. **86**, 1085 (1989).
[6]K. Attenborough and Y. Chen, J. Acoust. Soc. Am. **87**, 1010 (1990).
[7]L. Kelders, W. Lauriks, and J. F. Allard, J. Acoust. Soc. Am. **104**, 882 (1998).
[8]W. Lauriks, L. Kelders, and J. F. Allard, Wave Motion **28**, 57 (1998).
[9]J. F. Allard, G. Jansens, G. Vermeir, and W. Lauriks, J. Acoust. Soc. Am. **111**, 690 (2002).
[10]J. F. Allard, M. Henry, C. Glorieux, S. Petillion, and W. Lauriks, J. Appl. Phys. **93**, 1298 (2003).
[11]G. Belloncle, H. Franklin, F. Luppé, and J. M. Conoir, Ultrasonics **41**, 207 (2003).
[12]L. Boeckx, P. Leclaire, P. Khurana, C. Glorieux, W. Lauriks, and J. F. Allard, J. Acoust. Soc. Am. **117**, 545 (2005).
[13]T. Pritz, J. Sound Vib. **81**, 359 (1982).
[14]T. Pritz, Appl. Acoust. **60**, 279 (2000).
[15]M. A. Biot, J. Acoust. Soc. Am. **28**, 168 (1956).
[16]M. A. Biot and D. G. Willis, J. Appl. Mech. **24**, 594 (1957).
[17]D. L. Johnson, J. Koplik, and R. Dashen, J. Fluid Mech. **176**, 379 (1987).
[18]D. Lafarge, P. Lemarinier, J. F. Allard, and V. Tarnow, J. Acoust. Soc. Am. **102**, 1995 (1997).
[19]W. M. Ewing, W. S. Jardetsky, and F. Press, *Elastic Waves in Layered Media* (McGraw-Hill, New York, 1957).
[20]D. Royer and E. Dieulesaint, *Elastic Waves in Solids: Free and Guided Propagation* (Springer, Berlin, 1999), Vol. 1.
[21]L. Boeckx, P. Leclaire, C. Glorieux, W. Lauriks, and J. F. Allard, Measuring the Dynamic Shear Modulus of Poroelastic Foams in the Audible Frequency Range, Proceedings of the 18th International Congress on Acoustics, Kyoto, Japan, 4–9 April 2004 (unpublished).
[22]L. Kelders, J. F. Allard, and W. Lauriks, J. Acoust. Soc. Am. **103**, 2730 (1998).
[23]J. F. Allard, M. Henry, L. Boeckx, P. Leclaire, and W. Lauriks, J. Acoust. Soc. Am. (to be published).